



A Simple Mathematical Model of Second-Messenger Mediated Slow Excitatory Postsynaptic Potentials

P.P. BERTRAND, E.A. THOMAS, W.A.A. KUNZE, AND J.C. BORNSTEIN

*Department of Physiology and Department of Anatomy and Cell Biology,
University of Melbourne, Parkville 3052, Australia*

p.bertrand@physiology.unimelb.edu.au

Received July 13, 1998; Revised April 7, 1999; Accepted June 7, 1999

Action Editor: Christof Koch

Abstract. We have developed a novel and simple mathematical model of a slow excitatory postsynaptic potential (EPSP) based on an abstraction of the processes of activation, inactivation, and summation of a cAMP, protein kinase A (PKA)-dependent second-messenger cascade. The model describes the activation of receptors, G-proteins, and production of cAMP as the first stage and uses first-order, non-rate-limited kinetics. The second stage corresponds to the release of active, PKA catalytic subunit and can use first- or higher-order kinetics. The third stage represents simple phosphorylation of ion channels and is limited by the number of channels available. The decay of each stage is based on first-order, mass-action kinetics. These equations and some variations were solved numerically and values of the parameters were determined by fitting to a variety of experimental data from myenteric neurons of the guinea-pig ileum. The model produced a slow EPSP with a nonlinear stimulus-response relationship that resulted from the underlying kinetics of the signaling cascade. This system of equations is suitable for incorporation into a large-scale computer simulation, and the methodology should be generalizable to other pathways.

Keywords: computer simulation, slow synaptic transmission, enteric reflexes

1. Introduction

G-protein coupled receptors control many complex intracellular phenomena including gating of membrane bound ion channels and activation of protein kinases (Ross, 1989, Hille, 1992). Control can be exerted directly, by G-protein subunits, or through diffusible second messenger systems such as the cAMP/protein kinase A (PKA) system (Ross, 1989, Gray et al., 1998). In the latter case, the original biological signal may be significantly amplified and its time course extended (Torre et al., 1995).

In the enteric nervous system (ENS)—the intrinsic nervous system found within the wall of the intestine—second-messenger mediated slow excitatory postsynaptic potentials (EPSPs) (see Fig. 1) can be differ-

entiated from nicotinic fast EPSPs by their long time course (>5 s), long latency (>100 ms), and nonlinear summation (Wood, 1994). The long duration and nonlinear summation imply that dramatic, long-lasting changes may be made in the behavior of an individual neuron and that changes to many such neurons may underlie complex behavioral changes in the whole organ. Recent pharmacological evidence supports this role of the slow EPSP by demonstrating slow synaptic transmission from sensory neurons to interneurons in both the ascending and descending components of the peristaltic reflex (Johnson et al., 1998).

To study further the role that slow EPSPs may play in the control of the whole intestine, the activities of large groups of enteric neurons need to be studied simultaneously. One technique that facilitates this type

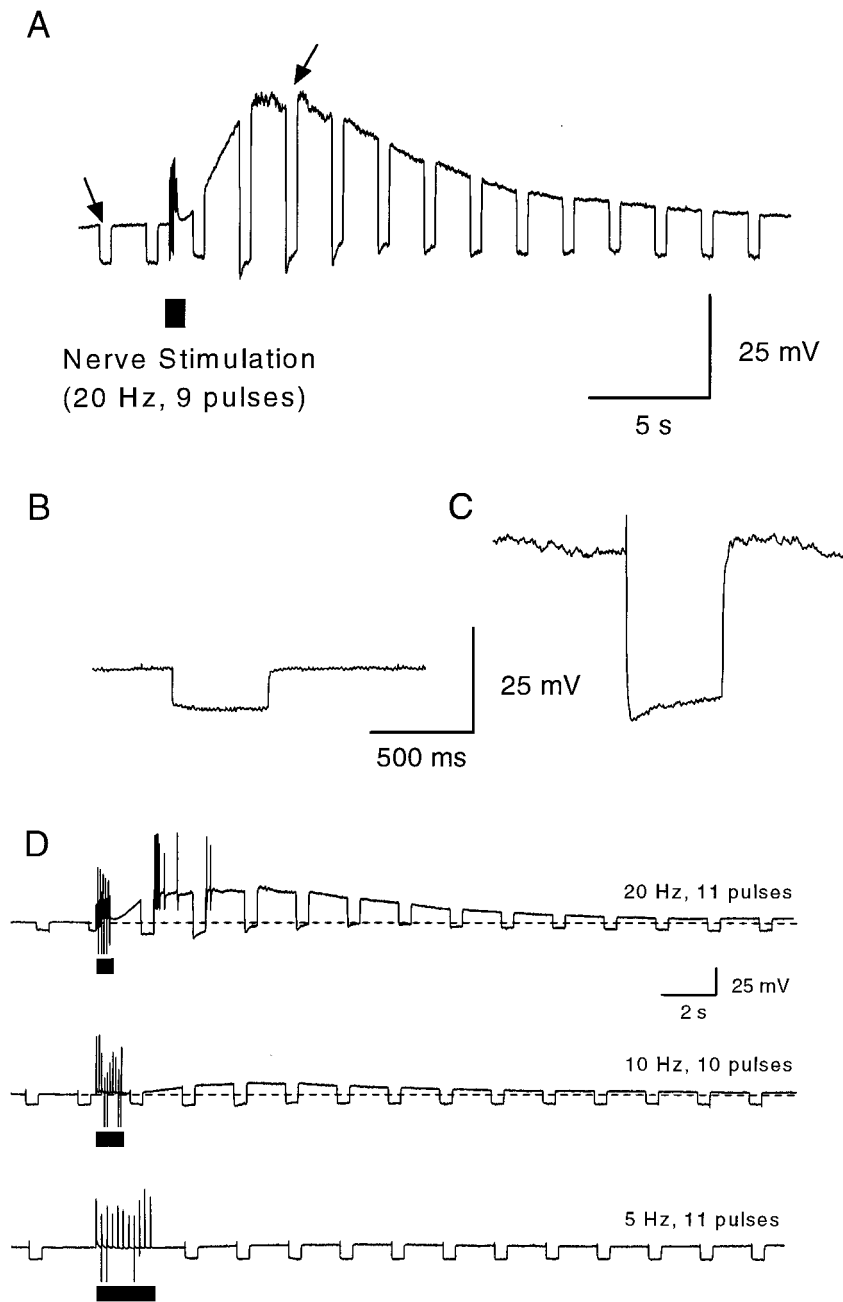


Figure 1. This figure shows a voltage trace of a slow EPSP obtained from an intracellular voltage recording from a myenteric neuron. **A:** The complete time course of the slow EPSP is shown. The downward deflections in the voltage trace are due to hyperpolarizing current pulses passed through the recording electrode every 2 sec. to measure the input resistance of the cell before and during the slow EPSP. Stimulation of the presynaptic nerve fibers are indicated by the solid bar; note the stimulus artifacts. The arrows indicate the positions from which the enlarged traces in B and C were taken. **B:** The voltage deflection in response to a -100 pA current pulse before initiation of the slow EPSP. The small voltage deflection shows that the resistance is low. **C:** An identical hyperpolarizing current pulse given near the peak response of the slow EPSP. The resistance is high; this coupled with the large depolarization indicates that a potassium conductance has decreased. Note that the sag seen in the voltage deflection is due to an I_H . **D:** Slow EPSPs elicited by 10 or 11 pulse stimuli at 5, 10, and 20 Hz in the same neuron, the dashed line indicates the position of the resting membrane potential (approximately -70 mV). As the stimulus frequency is increased from 10 to 20 Hz, there is a large increase in amplitude of slow EPSP. The upward deflections at the peak of the 20 Hz slow EPSP are truncated action potentials. Compared to other neurons, this neuron required higher stimulus intensities to evoke a slow EPSP (see Fig. 6).

of study is computer simulation. Individual enteric neurons can be modeled, and the role that the slow EPSP has in controlling their behavior can be studied. Unfortunately, many of the biochemical processes that underlie the generation of slow EPSPs in enteric neurons are only known in general; thus a model of the slow EPSP would have many unknown parameters and weak predictive powers. However, by constructing a model that encapsulates the current knowledge of the system and simplifies it, a smaller number of parameters can be generated. These parameters can then be set by comparing the output of the model to experimental data. A simplified model will also run economically enough to be incorporated into a large-scale simulation of the ENS (Bornstein et al., 1997), thus allowing the role of the slow EPSP to be explored in the context of an intact neural circuit.

The first aim of this study is to produce a robust deterministic model of the activation, inactivation, and summation of second-messenger mediated slow EPSPs in enteric neurons. The second aim is to ensure that the resulting model is simple enough to be incorporated into a network simulation of tens of thousands of neurons. To achieve the former aim, we derived a system of equations based as closely as possible on the physical processes underlying generation of the slow EPSP. To meet the latter aim, we simplified the equations as follows. First, the simplest kinetics that produced a realistic output were used (Destexhe et al., 1994). Second, all diffusion was ignored. Finally, multiple, short-time-scale events, on the order of 100 times faster than the output of the model, were collapsed into single events (Destexhe et al., 1994; Lamb, 1996).

1.1. Background

The initial motivation for this study was to improve an existing model of the slow EPSP used in a large-scale computer simulation of the ENS in the guinea-pig small intestine (Bornstein et al., 1997). Myenteric neurons—which are primarily responsible for the movements of the intestine, such as the complex motor behaviors that occur during peristalsis (Furness and Costa, 1987)—were studied. The interactions between sensory neurons and higher-order neurons are known to be, at least in part, via slow EPSPs (Kunze et al., 1993). These events are well characterized in terms of the neural input required to generate them, and their importance in reflexes is well documented, although not fully understood (Kunze and Furness, 1999). In the Bornstein

et al. (1997) study, slow synaptic input drove an internal stage, representing a concentration of a diffusible, second messengerlike substance. Once the internal stage exceeded a given threshold, the conductance change underlying the slow EPSP was triggered. The value of the internal stage followed a fixed time course for each synaptic event and was summed linearly for multiple events. The conductance change on the other hand was an all-or-nothing response in that it was independent of the exact nature of the input and further input events did not summate. These simulations demonstrated that transmission via slow EPSPs could explain the latencies of reflex responses evoked by physiological stimuli. The simulation also predicted that transmission of this sort would produce a high degree of temporal correlation in firing between neurons well away from the stimulus area (Bornstein et al., 1997, Thomas et al., 1999). However, this correlation might be explained by the lack of graded responses in both the onset and amplitude of the slow EPSP. To test further whether correlated output is a real network property, a more physiologically realistic model of the slow EPSP is required.

1.2. The Slow EPSP in Myenteric Neurons

Several slow EPSPs evoked in a single myenteric neuron are shown in Fig. 1. The slow EPSP in Fig. 1A was evoked by a 1 sec, 20 Hz, train of stimuli to the presynaptic nerve fibers. In general, slow EPSPs in myenteric neurons can be evoked by brief trains of 1 to 40 Hz stimulation (as in Fig. 1C–D), have a long latency (>100 ms), and have long duration (seconds to minutes) (Morita and North, 1985). For increasing numbers of presynaptic stimuli at a fixed frequency or for a fixed number of stimuli at increasing frequencies, the amplitude of the slow EPSP will initially increase, but eventually reach a plateau, typically resulting in a 10 to 20 mV depolarization (Morita and North, 1985). Under these same conditions, the duration of the slow EPSP will continue to increase (Clerc et al., 1999). The slow EPSP always significantly outlasts the stimulus period.

The depolarization associated with the slow EPSP is primarily due to closure of resting potassium conductances (g_K and $g_{K,Ca^{++}}$) (Akasu and Tokimasa, 1989; Bertrand and Galligan, 1994). There is strong evidence that slow EPSPs are mediated by the mobilization of intracellular second messengers that, ultimately, cause the observed changes in membrane

conductances. Tachykinins, such as substance P, mimic the slow EPSP (Katayama and North, 1978; Morita and Katayama, 1992; Galligan et al., 1987) and have been shown to cause accumulation of cyclic 3', 5' adenosine monophosphate (cAMP) (Baidan et al., 1992). Activators of adenylate cyclase, such as forskolin, also cause slow EPSP-like membrane depolarizations (Nemeth et al., 1986; Bertrand and Galligan, 1995). The receptors mediating the slow EPSP and the tachykinin responses are coupled through a pertussis toxin-insensitive G-protein (Bertrand and Galligan, 1995). The end point appears to be inhibition of g_K via a phosphorylation event (Bertrand and Galligan, 1995; Pan et al., 1997). Alternative pathways or interactions between G-proteins and second messengers are also supported by some of these data (Bertrand and Galligan,

1995; Ross, 1989; Clapham and Neer, 1997) but are poorly described; thus, we have not modeled them here.

2. Methods

2.1. The Model

The major components of the pathway that we modeled are illustrated in Fig. 2. After activation of the receptor, three distinct stages can be identified. The first stage, depicted on the left (Fig. 2, panel 1) starts with the activated G-protein coupled receptor and ends with the production of the second messenger, cAMP. The second stage, in the middle, relates only to the activation of protein kinase A, while the final stage, on the right,

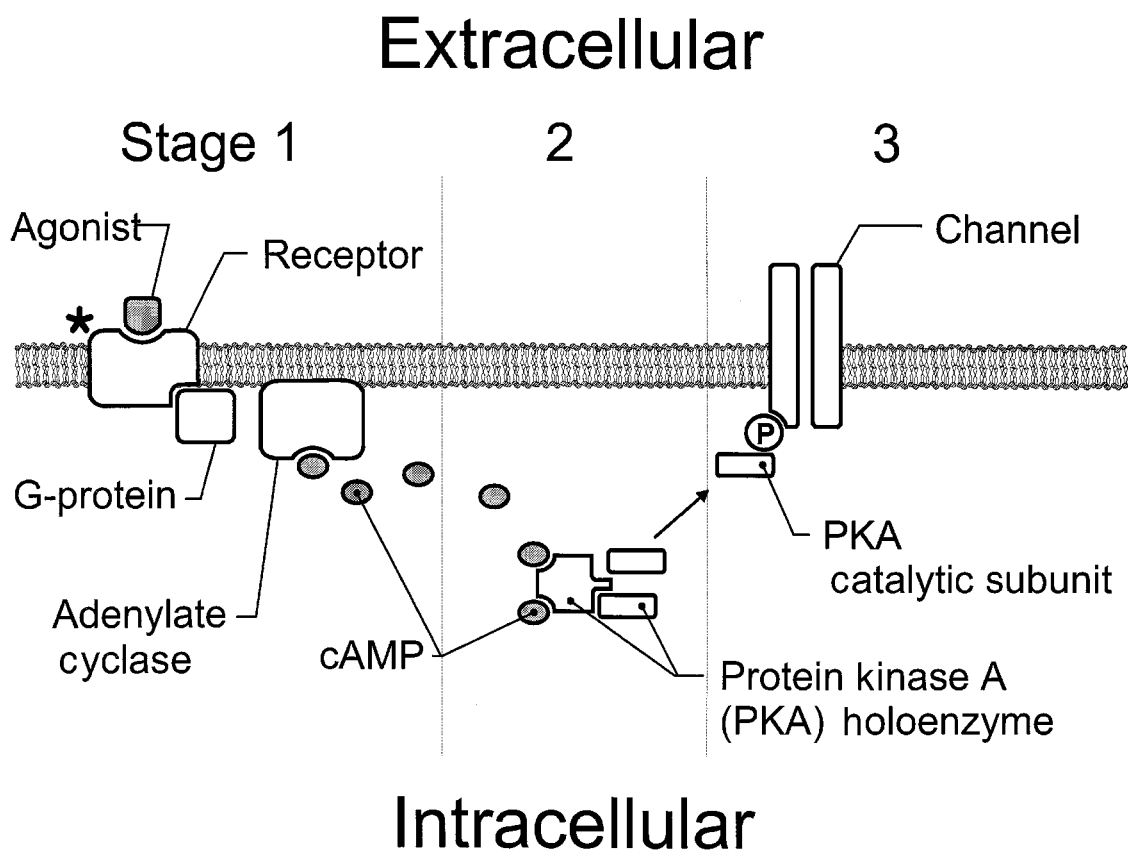


Figure 2. A schematic of the major steps involved in the cAMP second-messenger system believed to be responsible for the slow EPSP in myenteric neurons. **Stage 1** (panel 1): Agonist binds to the receptor and activates it (denoted by the *). The activated receptor then activates membrane-bound G-proteins that dissociate and activate adenylate cyclase, which then catalyses the production of cAMP. **Stage 2** (panel 2): Several molecules of cAMP bind to the protein kinase A (PKA) holoenzyme, which releases two catalytic subunits. **Stage 3** (panel 3): The catalytic subunits phosphorylate channels (indicated by the P) and decreases their probability of opening.

relates to the phosphorylation and closure of a potassium channel.

2.2. The Model Input

The release of transmitter from the presynaptic nerve terminal, its diffusion across the synaptic cleft, and its binding to the receptor are not modeled *per se* but are described by the function, $L(t)$. When the input is individual synaptic events, the amount of time that the agonist is present and bound to receptor is very small compared to the time course of the slow EPSP so the shape of $L(t)$ does not matter and can be approximated as a series of Dirac delta functions (Bennett and Gibson, 1995; Destexhe and Sejnowski, 1995). For example, for a series of action potentials occurring at times $\{t_i\}$

$$L(t) = \sum_i \rho_i \delta(t - t_i), \quad (1)$$

where ρ_i would represent relative synaptic strengths, absolute synaptic strength can be scaled into the final parameter α (see below).

2.3. First Stage

The first stage of the model describes the linear production and removal of cAMP (Fig. 2, panel 1). The slow rate of production and removal of cAMP dominates the kinetics of this stage, thus the early reactions in the cascade are not included. Reactions involving cAMP typically last many seconds (Buxbaum and Dudai, 1989; Hille, 1992; Hempel et al., 1996) while those involving activation of G-proteins often last only tens to hundreds of milliseconds (Lamb, 1996; Torre et al., 1995). The receptor activates the G-protein, which can inactivate quickly. We assume both the receptor and the G-protein inactivate independently of other substances and with first-order kinetics. The rate of production of cAMP is proportional to the amount of active adenylate cyclase, which, in turn, is proportional to the amount of activated G-protein. Thus, the linear rate of activation of receptor leads directly to the linear rate of cAMP production. As with diffusion of transmitter, the diffusion of cAMP is not modeled. The cAMP is removed by the actions of a cAMP phosphodiesterase (PDE). We have assumed that the rate of removal of cAMP is proportional to the amount of cAMP present (see Discussion). This leads to the equation

$$\frac{dD}{dt} = \alpha_1 L(t) - \beta_1 D, \quad (2)$$

where D is the amount of diffusible second messenger (i.e., cAMP), $L(t)$ is the amount of agonist, α_1 is the rate constant for production of D , and β_1 is the rate constant for the removal of D .

2.4. Second Stage

The second stage of the model covers events following the production of cAMP through to the activation of PKA (Fig. 2, panel 2). The PKA holoenzyme is composed of two tightly bound regulatory subunits and two catalytic subunits. In this instance, we use second-order kinetics as an approximation of the interactions of two molecules of cAMP on each of the two regulatory subunits (Buxbaum and Dudai, 1989) (see Model Variations, below). Furthermore, the amount of cAMP is assumed to be small compared to the amount of PKA, and so the reaction is not limited by the amount of PKA. Thus, the rate of accumulation of the disassociated catalytic subunit is proportional to the square of the amount of second messenger. The catalytic subunits rebind with PKA independently, and hence their rate of removal is assumed to be proportional to the amount of catalytic subunit present (see Discussion). This leads to

$$\frac{dC}{dt} = \alpha_2 D^2 - \beta_2 C, \quad (3)$$

where C is the amount of catalytic subunit (the second stage reactant), α_2 is the rate constant for the production of the catalytic subunit, and β_2 is the rate constant for the removal of C .

2.5. Third Stage

The final stage of the model describes phosphorylation of potassium channels (Fig. 2, panel 3). A simplification was made by assuming that the channel has only one phosphorylation site and that phosphorylation causes a direct transition from an open conducting state to a closed nonconducting state (see Discussion). The rate of phosphorylation is proportional to both the amount of catalytic subunit and to the amount of unphosphorylated channel. Thus the reaction is rate limited by the number of channels available. The rate of dephosphorylation of the channel protein (which is carried out by protein phosphatases) is assumed to be proportional to the number of phosphorylated channels. Any variation in the activity of protein phosphatases

has not been modeled as a part of this system. This gives

$$\frac{dP}{dt} = -\alpha_3 C P + \beta_3 (1 - P), \quad (4)$$

where P is the relative amount of unphosphorylated channel, α_3 is the forward rate constant, and β_3 is the rate constant at which channels return to the unphosphorylated state. The total conductance is simply the product of the maximum conductance and the relative amount of open channel.

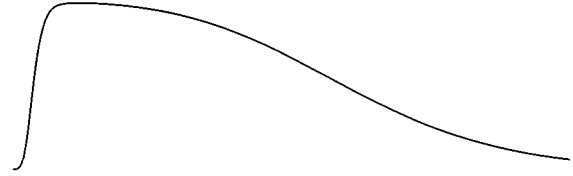
If the total conductance change is small compared to the total membrane conductance and there are no other active conductance changes, then the relative voltage change, r , will be equal to $1 - P$. In general, the conductance change is large compared to the passive membrane resistance (see Fig. 1), so $r < 1 - P$. But as the slow EPSP evolves, voltage dependent conductances increase, and other non-cAMP pathways also increase conductances (Bertrand and Galligan, 1994), which serve to increase the estimate for r . Thus, in what follows $r = 1 - P$. This produces better fits than calculating r assuming no other conductance changes.

Although the model has three forward rate constants, $\alpha_{\{1,2,3\}}$, the third stage, $P(t)$, depends only on the combination $\alpha_1 \sqrt{\alpha_2 \alpha_3}$. Furthermore, only the third stage will be fitted to data so redundant parameters can be eliminated. Therefore, we make the following substitutions—

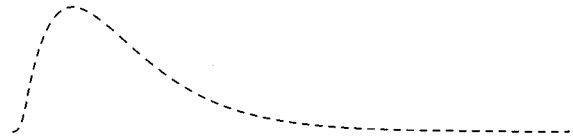
$$C \rightarrow \frac{C}{\alpha_3}, \quad D \rightarrow \frac{D}{\sqrt{\alpha_2 \alpha_3}}, \quad \text{and} \quad \alpha_1 \rightarrow \frac{\alpha}{\sqrt{\alpha_2 \alpha_3}} \quad (5)$$

—to remove α_2 and α_3 . This leaves four independent parameters— α , β_1 , β_2 , and β_3 . The first parameter can be thought of as a coupling constant, gain, or amplification factor. The three remaining parameters determine the rate of decay of the three stages. If no substance is present in the proceeding stages, then the i th stage will decay with a half-life given by $\ln(2)/\beta_i$. When no agonist is present, there is one equilibrium, which is stable, at $D = 0$, $C = 0$, $P = 1$ representing no substance in the first two stages and the channel protein completely unphosphorylated. The relationships between time courses of the three-stages are illustrated in Fig. 3; the seed parameter 0.1 was used.

Third (final) stage



Second stage



First stage



Input (10 pulses)



Figure 3. The relationship of the time-dependent change of the three stages of the model. The model input (bottom trace) is a train of 10 pulses at 10 Hz. The different stages are scaled arbitrarily. The third, and final, stage (top trace) represents the closure of potassium channels and is comparable to the waveform of the slow EPSP. The intermediate traces represent the time courses of the internal stages of the model (Stages 1 and 2), which were not directly compared to experimental data. All parameters used to generate these data were at the seed values of 0.1.

3. Results

3.1. Model Output

The equations derived above consist of three stages, with second-order kinetics in the second stage and first order kinetics in the others (three-stage, second-order). The output of these equations was characterized using values for the parameters obtained by fitting an experimental dataset (see below) (Morita and North, 1985). In Fig. 4, various patterns of fixed frequency or number of synaptic inputs are shown. Figure 4A shows a family of simulated slow EPSPs produced by fixed-duration stimuli but with varying numbers of pulses, while in

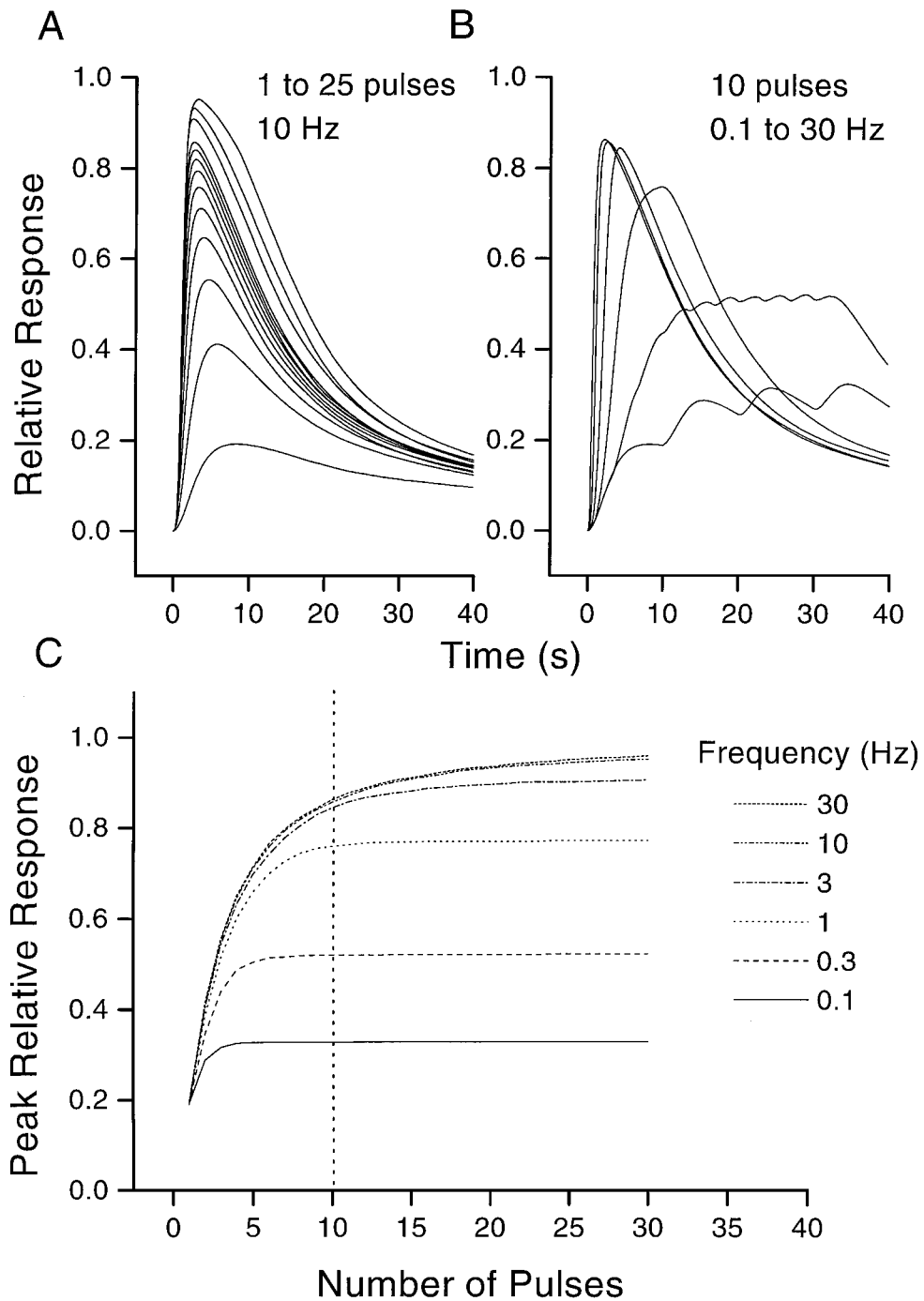


Figure 4. Waveforms generated by the model for a variety of inputs all with a fixed duration of 3 sec. **A:** Each waveform is a full time course response for a fixed frequency of 10 Hz and a variable number of pulses. The peak duration increases as a function of the number of pulses. The sequence illustrated is from 1 to 10 Hz and then 15, 20, and 25 Hz. **B:** Each curve is a full time course response for a fixed number of pulses (10) with different frequencies. The sequence illustrated is from 0.1 to 30 Hz in half log steps. The curve for 0.1 Hz has been truncated at the fourth pulse. **C:** Composite graph showing how the peak response changes as a function of the number of pulses (on the abscissa) and the frequency (different lines). Frequencies from 0.1 to 30 Hz and from 1 to 30 pulses are illustrated. The dotted line indicates the position into which data represented in panels A and B were incorporated. The parameters used to illustrate this figure are from a three-stage, second-order model, fit to the Morita and North (1985) data; $\alpha = 0.30\text{s}^{-1}$, $\beta_1 = 0.51\text{s}^{-1}$, $\beta_2 = 0.73\text{s}^{-1}$, and $\beta_3 = 0.18\text{s}^{-1}$. These data also appear in Table 1.

B the simulated slow EPSPs are produced in response to varying durations of the train of stimuli but with the number of pulses held constant. Figure 4C show stimulus response curves with the peak amplitude of the simulated slow EPSP plotted versus the number of pulses for a range of frequencies.

3.2. Comparison to Experimental Data

We examined the ability of the model to reproduce experimental data from two independent datasets. The first was from Morita and North (1985), which consisted of peak relative response and time to half decay data for a variety of fixed-frequency inputs in myenteric S neurons. The second dataset was generated for this study and consisted of the complete time courses of slow EPSPs from 7 myenteric S neurons.

3.3. Methods

For both datasets the input $L(t)$ was approximated using Eq. (1) with $\rho_i = 1$. The first differential equation was solved analytically, and the remaining stages solved using the fourth-order Runge-Kutta method with adaptive time step (Press et al., 1992). Fitting parameters to data required minimization of an error term (see below); these minimizations were performed using Powell's algorithm (Press et al., 1992). All fitting parameters were seeded at a value of 0.1; values of greater than 1 seemed to cause the fitting session to become unstable, with all parameters increasing indefinitely. In general, the solution to Eqs. (2) to (4) involves complex combinations of exponential terms for which the three time constants need to be determined. This is a difficult problem (Acton, 1970), which is characterized by being computationally expensive to solve and by generating a wide range of parameters that fit the data almost as well. Codes were written in the C programming language. Data for Figs. 3 and 4 were generated using the Linux version of Octave 2.0.5, which uses the LSODE package for differential equation integration. Octave is freely available from the Internet at <http://www.che.wisc.edu/octave/>. Source code and data used in this study are available over the Internet from <http://dirac.physiology.unimelb.edu.au/pdg/slowepsp/>.

For the peak relative response and time to half decay from Morita and North (1985), the error term was calculated as follows: for each observation (that is, for

a given stimulus) in the experimental dataset, Eqs. (2) to (4) were solved (as in Fig. 4), and the relative peak response and time to half decay were extracted (as in Fig. 5). The error, as a function of the parameter set $(\alpha, \beta_1, \beta_2, \beta_3)$, was then calculated as

$$E(\alpha, \beta_1, \beta_2, \beta_3) = \sum_i \left(\frac{\tau_i - \tau(s_i, \alpha, \beta_1, \beta_2, \beta_3)}{\tau_i} \right)^2 + \sum_i \left(\frac{r_i - r(s_i, \alpha, \beta_1, \beta_2, \beta_3)}{r_i} \right)^2, \quad (6)$$

where s_i represents the i th stimulus, τ_i and r_i represent the observed times to half decay and peak responses, and $\tau(\cdot)$ and $r(\cdot)$ represent the model predictions for a particular parameter set. Since the two error terms are normalized, they give approximately equal contribution to the error. This summed value represents the "goodness of fit" for the current values of the parameters.

The individual trace data from seven neurons were defined by a sequence of n experimental points, $\{t_i, V_i\}$. The error, as a function of the parameter set $(\alpha, \beta_1, \beta_2, \beta_3)$, was then calculated as

$$E(\alpha, \beta_1, \beta_2, \beta_3) = \sum_i \left(\frac{V_i}{V_{\max}} - r(t_i, \alpha, \beta_1, \beta_2, \beta_3) \right)^2, \quad (7)$$

where $V_{\max} = \max V_i$ and $r(\cdot)$ is the model prediction for a given time and parameter set.

3.3.1. Fitting the Peak Response and Half Life-Dataset. The data of Morita and North (1985) represents the most thorough investigation into the input and output relationship for slow EPSPs in the ENS. Their protocol consisted of evoking slow EPSPs with a constant frequency stimuli in the range of 1 to 30 Hz with a train duration of 3 sec. Stimulus pulse duration and voltage were held constant. Figure 5 shows how the maximum amplitude and the time to half decay are defined. In general, slow EPSPs can show significant variation from cell to cell, and this is particularly apparent in the time to half decay data from Morita and North (1985).

The results of simultaneously fitting both the time to half decay and relative peak response data to a three-stage, second-order model are shown in Fig. 6 (see below, Model Variations). The parameter values found

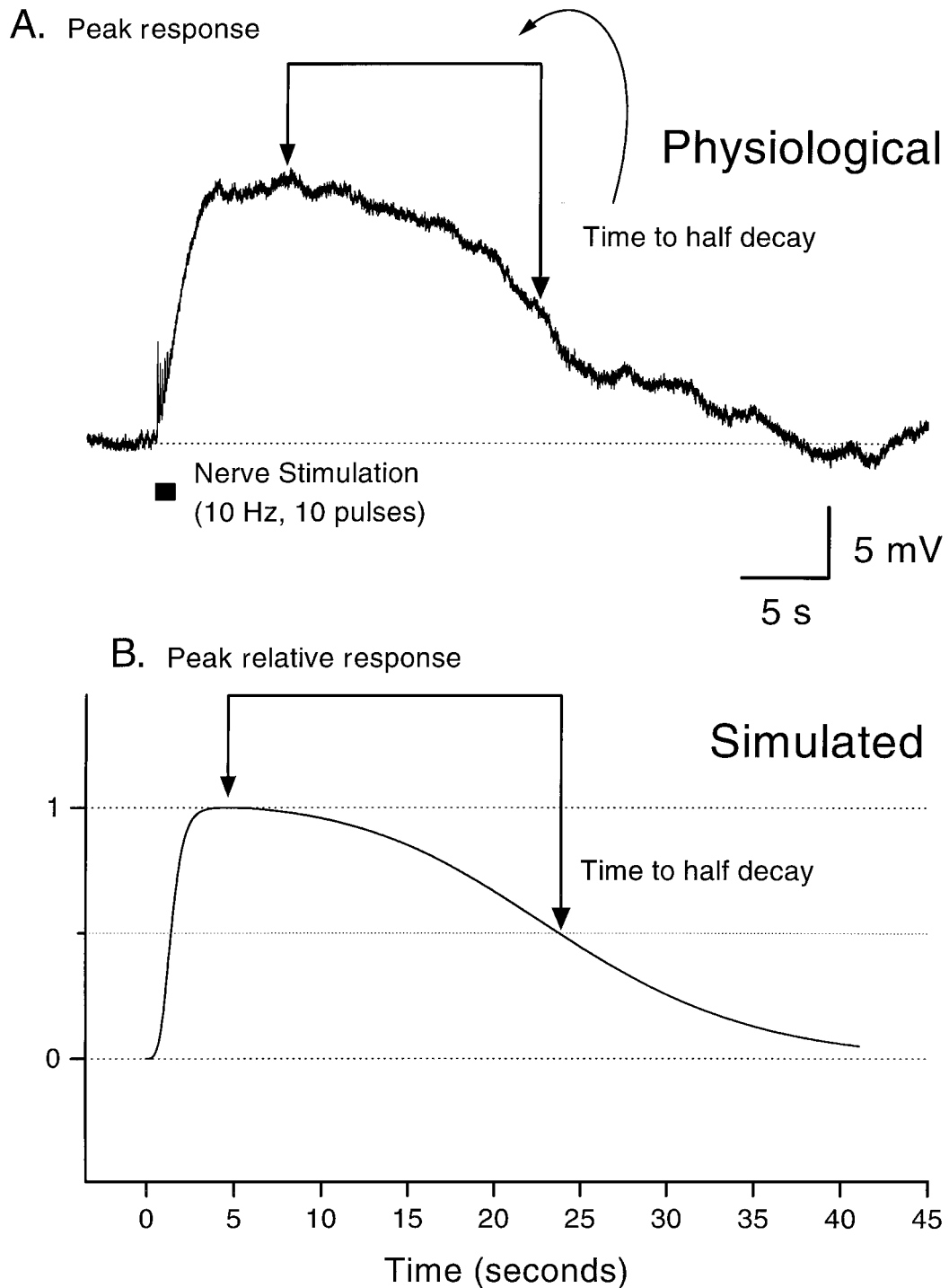


Figure 5. Features of the slow EPSP that were fitted by the model. **A:** A voltage trace from a myenteric neuron showing a slow EPSP evoked by stimulation presynaptic nerve fibers (at the bar), note the stimulus artifacts in the voltage trace. The peak amplitude and time to half-decay (as measured from the peak) of the slow EPSP are marked by the arrows. **B:** Simulated slow EPSP with the peak amplitude and time to half-decay marked by the arrows. The parameters derived for this fit for a three-stage, second-order model were $\alpha = 0.17s^{-1}$, $\beta_1 = 0.19s^{-1}$, $\beta_2 = 0.38s^{-1}$, and $\beta_3 = 0.21s^{-1}$. These data are part of the average data in Table 1. Interestingly, two other slow EPSPs from this cell were fit by very similar parameters.

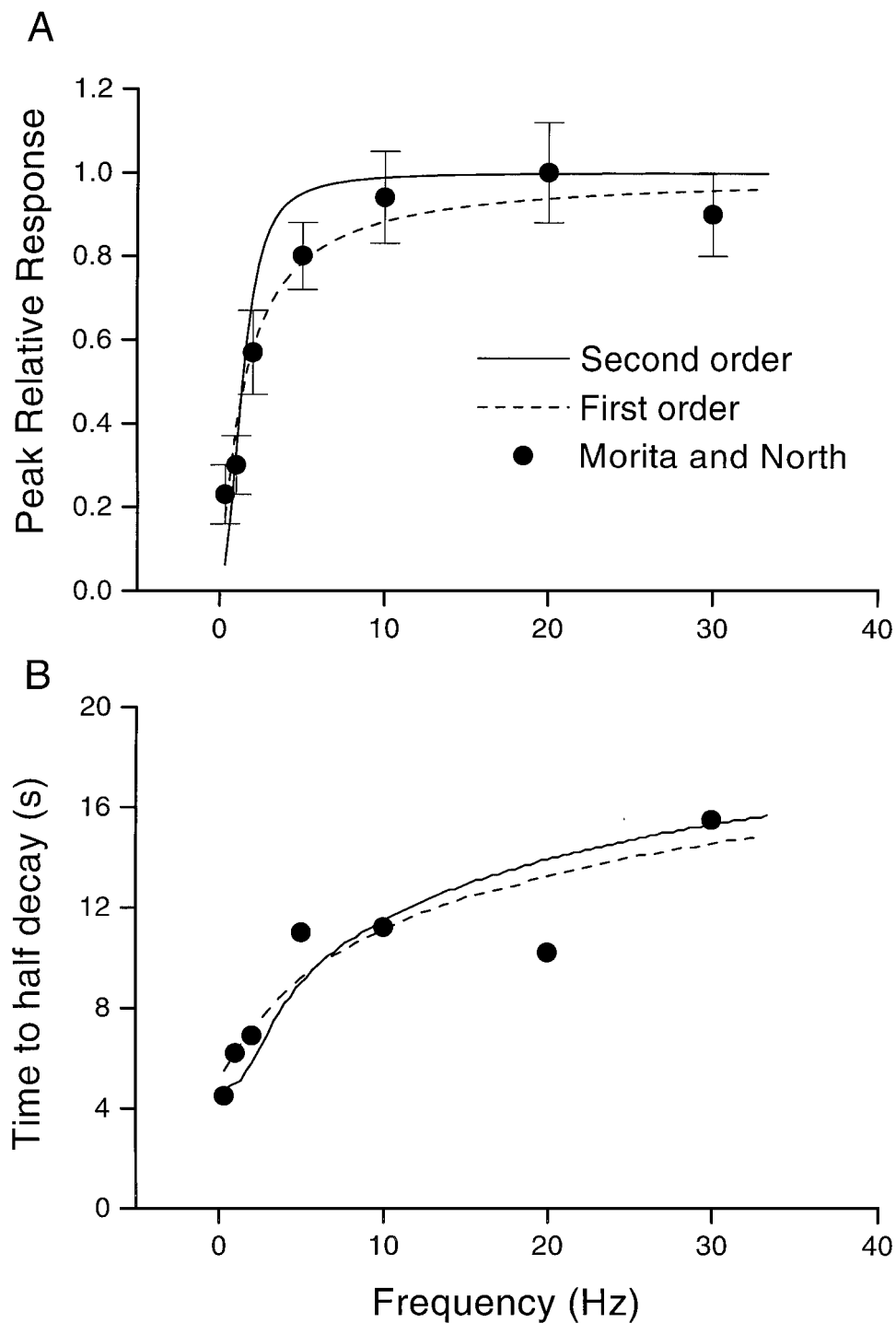


Figure 6. Real data were used to calibrate the internal parameters. Data from studies by Morita and North (1985) (shown in the filled circles) consisted of the peak response and time to half decay of the slow EPSP for a range of stimulus frequencies. These data were fit using a least-squares, error-minimization method. Best fits using first- and second-order kinetics in the second stage are shown (with the dashed and solid lines, respectively). In both graphs the abscissa is the frequency for a 3 sec. stimulus pulse. **A:** Peak relative amplitude. Both models fit these data well, but the three-stage, second-order model showed a tendency to saturate more quickly. **B:** Time to half-decay (seconds). Both models fit these data well.

Table 1. The final parameters ($\alpha, \beta_{\{1,2,3\}}$) in sec^{-1} , for the Morita and North (1985) data (MN) and for the average trace data (TR) for the three-stage model with either first- (3/1) or second- (3/2) order kinetics in the second stage. Parameters for TR are averages from seven neurons.

	3/1 TR	3/1 MN	3/2 TR	3/2 MN
α	0.28	0.11	0.22	0.30
β_1	0.37	0.54	0.41	0.51
β_2	0.28	0.47	0.27	0.73
β_3	0.13	0.24	0.12	0.18

for the curves shown are $\alpha = 0.30 \text{ s}^{-1}$, $\beta_1 = 0.51 \text{ s}^{-1}$, $\beta_2 = 0.73 \text{ s}^{-1}$, and $\beta_3 = 0.18 \text{ s}^{-1}$; these data also appear in Table 1. The last three parameters are the decay constants for the three stages. The fact that they are all within an order of magnitude of each other indicates that the kinetics of at least three stages seem to be important in determining the overall properties of the system. The first parameter, α , is an amalgam of many physical parameters and so does not have a direct interpretation; it is proportional to the time the agonist spends bound to the receptor, to a term involving the forward rate constants for each of the three stages, and to the amount of agonist released at each connection.

3.3.2. Fitting Full-Time Course Data. The equations were also fitted to a second set of data, a limited number of slow EPSPs from seven myenteric S neurons whose stimulus parameters and time courses were determined experimentally for this study (see Bertrand and Galligan, 1994), for details of electrophysiology). In each case, the stimulus was a 1 sec. train of identical pulses applied to an internodal nerve strand at 10 Hz. These slow EPSPs showed a two- to three-fold variation in time to half decay, with a much smaller variation in peak amplitude and in the time to peak. Fitting was carried out as follows. Because the recorded waveforms included membrane events, such as action potentials, fast EPSPs, and responses to current injections, a few points (13 to 25), including a point at, or near, the peak response, were manually extracted from each trace at times when no obscuring event occurred. To allow calculation of error terms, these data were then converted to relative responses and normalized to 1. The fitting was then carried out as described in the methods section.

Figure 7 shows an example of two slow EPSPs, each of which has been fitted by the model (including those

Table 2. The final parameters ($\alpha, \beta_{\{1,2,3\}}$) in sec^{-1} , for individual trace data (TR) for a three-stage model with second- (3/2) order kinetics in the second stage. The means and standard deviations (STD) for each parameter are listed at the bottom.

	α	β_1	β_2	β_3
1	0.15	0.14	0.28	0.18
2	0.16	0.26	0.26	0.05
3	0.46	0.55	0.36	0.18
4	0.08	0.12	0.21	0.10
5	0.19	0.22	0.24	0.10
6	0.17	0.19	0.38	0.21
7	0.31	1.38	0.18	0.04
Mean	0.22	0.41	0.27	0.12
STD	0.13	0.45	0.07	0.07

from Model Variations), and the parameters used. In general, the three-stage, second-order model can be well fitted to the decay phase of the recorded waveform. This is not surprising as the decay phase in the model is largely controlled by three rate constants, $\beta_{\{1,2,3\}}$. The model is not always able to match the time to peak of the waveform, or the rate of rise. This is because the rising phase is controlled by a single rate constant, α , which also controls how much second messenger is generated in the first stage and hence the peak response. The parameters for all of the traces averaged together can be found in Table 1 (including those from—Model Variations), while parameters for the individual traces are in Table 2. Interestingly, the final parameters for the three stage, second order model on the Morita and North dataset and on the full time course dataset are very similar, with a substantial difference only in the value of β_2 .

3.4. Model Variations

In the second stage of the model (which is described by Eq. (3)), second-order kinetics are used because two to four molecules of cAMP must bind simultaneously to the PKA regulatory subunits before the catalytic subunits are released (Builder, 1980; Buxbaum and Dudai, 1989). We wished to determine the importance of this decision by comparing a three-stage, first-order model to the results obtained with the three-stage, second-order model (above). When fitted to individual waveforms from the full trace dataset, either model fit the data equally well (not shown). However, it might be expected that the order of the kinetics will

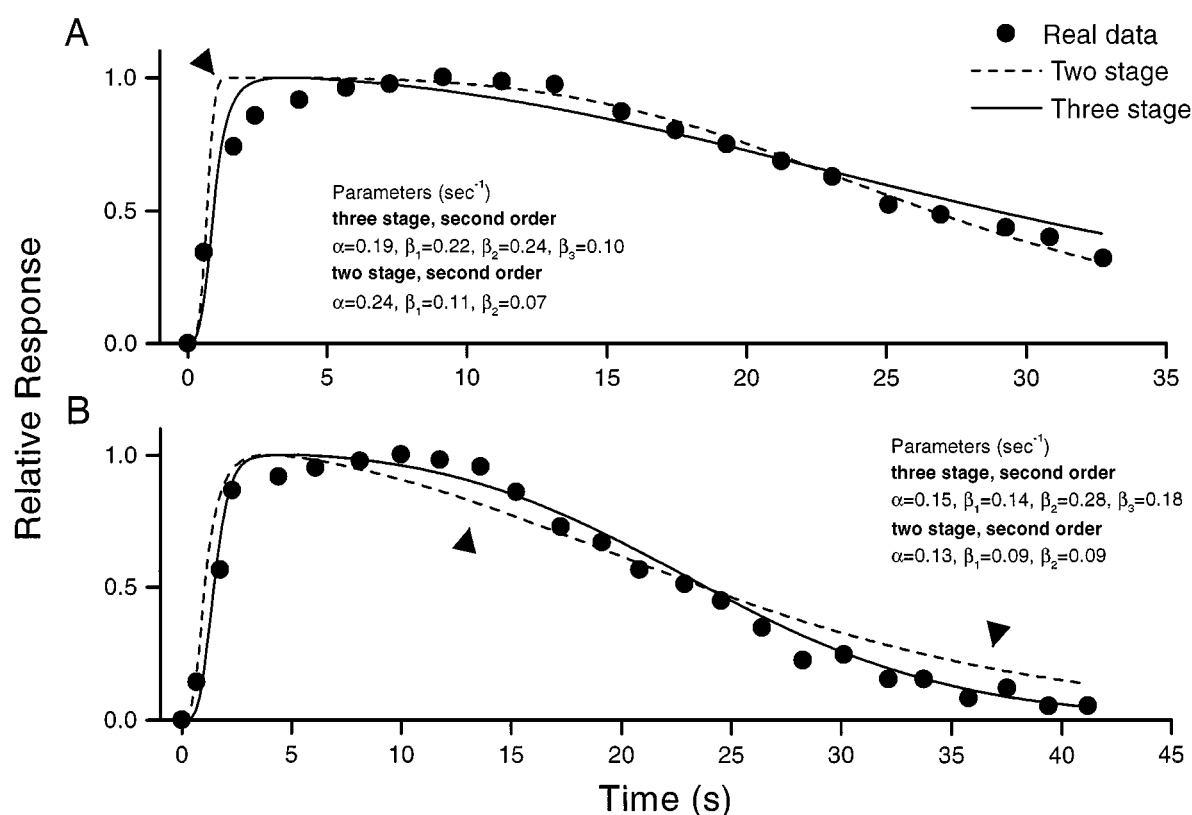


Figure 7. Graphs showing the output of the model fitted to two slow EPSPs from different enteric neurons; seven neurons were fitted in all. Output from a two-stage model, Eq. (9), is shown in the dashed line, and the three-stage model, Eqs. (2) to (4) is shown in the solid line. The experimental data are shown as the filled circles. Only a small number of points from the recorded waveforms were used in the fitting process. The parameters derived for each fit are shown near the trace; these data are part of Tables 1, 2, and 3. **A:** In some cases the two-stage model rose unnaturally quickly (arrow), apparently in an effort to match the decay phase of the recorded waveform. The three-stage model was more constrained and thus fit the rise and the decay reasonably well. **B:** Even when the rising phase of the two-stage model fit as well as the three-stage model, the decay phase was often poorly fit (arrows). Similar differences between the models were seen in the fits of the other five neurons.

be important in determining the stimulus response relationships. Figure 6 shows the comparison of first- and second-order kinetics in the second stage. Figure 6A shows that the first order kinetics are able to fit the data better, especially for stimuli of intermediate strength, while the second order kinetics appear to have a larger range to the peak response. Figure 6B shows that both first- and second-order kinetics are able to fit the time to half decay data equally well. The final parameters (shown in Table 1) for each model are also quite similar, with the largest differences in the values of α and β_2 , as would be expected.

In writing down Eqs. (2) to (4) many assumptions were made about which reactions could be treated as single steps. Equations with more than three stages

were not considered as this would introduce extra parameters. More parameters should make fitting the experimental data easier, but the model might then become too dependent on the data and thus have weaker predictive powers. A one-stage system was also rejected immediately because in this case the agonist must interact with the channel through a number of very rapid intermediate steps and, as soon as the agonist is no longer present, channels will start to reopen—that is, the system would have no memory. This is not compatible with the basic experimental observation that the peak response occurs well after the stimulus has ceased. A multistage system, on the other hand, “remembers” the stimulus as nonequilibrium concentrations of intermediate reaction products.

Table 3. The final parameters (α , $\beta_{1,2}$) in sec^{-1} , as in Table 1, for the two-stage model with either first- (2/1) or second- (2/2) order kinetics in the second stage. Parameters for TR are averages from seven neurons.

	2/1 TR	2/1 MN	2/2 TR	2/2 MN
α	0.14	0.18	0.14	0.34
β_1	0.19	0.34	0.10	0.29
β_2	0.07	0.23	0.08	0.20

A two-stage system, analogous to Eqs. (2) to (4), is

$$\begin{aligned} \frac{dD}{dt} &= \alpha_1 L(t) - \beta_1 D \\ \frac{dP}{dt} &= -\alpha_2 D^2 P + \beta_2 (1 - P). \end{aligned} \quad (8)$$

Note, the two stage model described above still incorporates the second order assumption (see above); a two-stage, first-order model was run (see Table 3) but qualitatively, was not able to fit any of the datasets (not shown). In general, the two-stage, second-order model was able to fit the peak response and half life data as well as the three stage, second order model (not shown), but was less able to fit some of the individual trace data. Figure 7 shows two examples where the two-stage, second-order model differed from the three-stage, second-order model. The two-stage model may rise too quickly (Fig. 7A) or overshoot on the decay phase (Fig. 7B). Alternately, the three-stage, second-order model may also have trouble with the complex decay phase (Fig. 7A).

4. Discussion

In this study, we have developed a model that describes the activation of a G-protein, cAMP/PKA pathway resulting in the phosphorylation of a potassium channel. A major finding is that important features of the signaling cascade can be abstracted out by a process of mathematical simplification, yet still produce a model capable of fitting a wide range of experimental data. Equally important is that more than one, though not all, of the models fit the data well.

4.1. Decay Phases of Stages 1 and 2

There were two assumptions about the decay phases of the first two stages that were incorporated into all of

the successful models. Where tested, models based on alternate assumptions failed to fit the data (not shown).

In the first stage, the decay is due to the hydrolysis of cAMP by a PDE. If this is described by Michaelis-Menton kinetics, then there are two simple approximations that can be made. The first is that the rate of decay is proportional to the amount of PDE and hence constant for positive D (cAMP). If this is true, then for large stimuli the half-life of the first stage will be linearly related to the stimulus size, and hence the total half-life of the output will be at least linearly related to the stimulus size. An examination of the Morita and North data (Fig. 6) shows that with increasing stimuli, the half-life increases less than linearly. Thus we chose to use the second approximation, that the decay is proportional to D .

The decay of the second stage is caused by the re-binding of two catalytic PKA subunits with the single, tightly bound pair of regulatory subunits. The simplest assumption is that the rate of decay is proportional to the square of the amount of catalytic subunit, C in Eq. (3), which leads to a $1/C$ decay. However, equations based on this assumption were not able to fit any of the datasets (not shown). An assumption that removal was linear gave the results presented. These data are not known for enteric neurons but can be justified by several known biochemical mechanisms such as an autoinhibition of the catalytic subunit (Taylor, 1989; Buxbaum and Dudai, 1989; Gray et al., 1998).

4.2. Evaluation of the Model

A three-stage model with either first-order or second-order kinetics in the second stage fits the dataset of Morita and North well, though with some qualitative differences (see Fig. 6), while both models fit the individual trace data with identical results (not shown). A two-stage or three-stage model with second-order kinetics in the second stage also fit the Morita and North data well, with the three-stage model having a minor advantage in the way it fit the slow rise and complex decay phases of the complete waveforms (Fig. 7). A two-stage model with first-order kinetics in both stages was unable to fit either dataset (not shown). It may be that this set of equations simply did not have the complexity necessary to fit the wave form of the slow EPSP.

Thus, any of the more complex systems of equations could prove useful in investigating slow EPSPs in large-scale simulations. To make stronger conclusions about which set of equations is better, it would be necessary

to obtain a series of slow EPSPs (similar to Fig. 1) from a large sample of cells that are receiving both synchronised and non-synchronised input. We leave this refinement for a future study.

4.3. *Other Models of G-Protein and Second Messenger Signaling*

A model similar to that of the present work is that of Naumoschat and an der Heiden (1997), which is based on receptor/G-protein interactions with the production of a generic second messenger as the final step. Their aim was to abstract out a system of general equations and determine their mathematical properties. Thus they did not include any reaction rates, nor did they fit their model to any data. Their process of abstraction and mathematical simplification is similar to the methodology used in the present study. In contrast, they include receptor/agonist complex desensitization and receptor sequestration via endocytosis, which we chose not to model to reduce complexity, in part because we were modeling several stages past the production of cAMP. There is evidence that receptor internalization occurs in myenteric neurons, though any effects of this in the current model will have been subsumed by the multiple decay phases (Southwell et al., 1996; Carman and Benovic, 1998).

Quite a different approach was taken in a model by Lamb and Pugh (1992), where the numbers of molecules and the rates for many of the reactions were known and diffusion was modeled as a stochastic process. The system studied was that of light transduction in the salamander rod cell (Lamb and Pugh, 1992; Lamb, 1996). Light is the agonist and rhodopsin molecules are G-protein coupled receptors which activate a cGMP PDE. While cGMP is present, ion channels are open; when light is present, the PDE is activated and concentrations of cGMP fall causing channels to close. This model matches experimental data very closely for the activation phase of the pathway, but does not incorporate an inactivation phase.

The model of Lamb and Pugh (1992) includes many real parameters for a tightly coupled system. For many other systems, not all these parameters are known, nor are the pathways involved as well characterized (Lamb and Pugh, 1992); slow EPSPs in myenteric neurons are a good example. Because the present study aimed to produce a model that would facilitate the investigation of large-scale neuronal interactions, we chose to use a more abstract approach (Lamb, 1996). In ad-

dition, our model was designed to handle situations where neurons receive complex, ongoing inputs, which last beyond the initial activation of the pathway; thus it was necessary to model the inactivation phase of the second-messenger system. The inactivation, or the return to the initial state, includes many more reaction rates that are not available for myenteric neurons or even for the salamander rod cell (Lamb and Pugh, 1992; Lamb, 1996).

A detailed model of $GABA_B$ receptor activation has been presented by Destexshe and Sejnowski (1995). Similar to the present study, they fit their model to biophysical data to derive parameters, and like Lamb and Pugh (1992) they explicitly modeled the movement of transmitter in the synaptic cleft. However, like the model of Naumoschat and an der Heiden (1997), they consider the pathway only one step beyond the G-protein, which in this case is a potassium channel. Their aim was to use their model to differentiate between proposed mechanisms underlying observed differences in $GABA_B$ and $GABA_A$ responses. One of their conclusions is that higher-order binding kinetics of G-protein to the potassium channel can account for significant nonlinearities in the $GABA_B$ stimulus response relationship (Destexshe and Sejnowski, 1995). Although the potassium channel modeled in the present study does not interact with G-proteins, it is interesting to note that the gating of the $g_K/g_{K,Ca^{++}}$ by phosphorylation presents a similar argument. Data on similar channels (see Vergara et al., 1998) suggest that they are all essentially tetramers. Thus, one may expect four (or more) sites for phosphorylation on the channel. As in Destexshe and Sejnowski, (1995), this could account for significant nonlinearities in the stimulus-response relationship of the slow EPSP that were not explored in this study.

Finally, a quantitative and detailed model of the activation of PKA by cAMP has been presented by Buxbaum and Dudai (1989). Although limited to one stage of the signaling cascade, their aim was to model the effects that changes in the ratio and in the state of phosphorylation of the catalytic and regulatory subunits have on production of cAMP. Like some of the previous models, extensive reaction data from wild-type and mutant *Drosophila* were used. This allowed them to correlate behavioral differences in mutants with differences in the activation of PKA and conclude that its long-term activation is important for memorylike functions. Unlike the model developed in this study, Buxbaum and Dudai (1989) modeled neither the

creation of cAMP from synaptic inputs nor the role of activated PKA at the single neuron level. Conversely, we used much of the same kinetic data as a starting point but then abstracted it out during development of the model.

5. Conclusion

We have demonstrated a method by which relatively general biochemical processes can be extracted from a complex system and, by fitting to experimental data, used to model specific pathways. The model created is mathematically simple and computationally efficient in both processor time and memory. The model can reproduce peak response and time to half decay data over a range of fixed frequency stimuli and so should be able to predict responses for more complex inputs. Future refinements of this system will include exploring the role of intracellular calcium and multiple phosphorylation events on the gating of the $g_K/g_{K,Ca^{++}}$.

Acknowledgments

We thank John Furness, Tricia Wright and the reviewers for their invaluable comments at various phases of writing this manuscript. This work was supported by National Institutes of Health DK 09162 (United States) and National Health and Medical Research Council 923211 (Australia).

References

- Acton SF (1970) Numerical Methods That Work. Harper & Row, New York.
- Akasu T, Tokimasa T (1989) Potassium currents in submucous neurones of guinea-pig caecum and their synaptic modification. *J. Physiol.* 416:571–588.
- Baidan LV, Fertel RH, Wood JD (1992) Effects of brain-gut related peptides on cAMP levels in myenteric ganglia of guinea-pig small intestine. *Eur. J. Pharmacol.* 225:21–27.
- Bennett MR, Gibson WG (1995) On the contribution of quantal secretion from close-contact and loose-contact varicosities to the synaptic potentials in the vas deferens. *Phil. Trans. Royal Soc. Lond.* 347:187–204.
- Bertrand PP, Galligan JJ (1994) Contribution of chloride conductance increase to slow EPSC and tachykinin current in guinea-pig myenteric neurones. *J. Physiol.* 481:47–60.
- Bertrand PP, Galligan JJ (1995) Signal-transduction pathways causing slow synaptic excitation in guinea pig myenteric AH neurons. *Am. J. Physiol.* 269:G710–G720.
- Bornstein JC, Furness JB, Kelly HF, Bywater RA, Neild TO, Bertrand PP (1997) Computer simulation of the enteric neural circuits mediating an ascending reflex: Roles of fast and slow excitatory outputs of sensory neurons. *J. Autonomic Nervous Sys.* 64:143–157.
- Builder SE, Beavo JA, Krebs, EG (1980) Stoichiometry of cAMP and 1,N6-etheno-cAMP binding to protein kinase. *J. Biol. Chem.* 255:2350–2354.
- Buxbaum JD, Dudai Y (1989) A quantitative model for the kinetics of cAMP-dependent protein kinase (Type II) activity. *J. Biol. Chem.* 264:9344–9351.
- Carman CV, Benovic JL (1998) G-protein-coupled receptors: Turn-ons and turn-offs. *Current Opinions in Neurobiol.* 8:335–344.
- Clapham DE, Neer EJ (1997) G protein $\beta\gamma$ subunits. *Ann. Rev. Pharmacol. and Toxicol.* 37:167–203.
- Clerc N, Furness JB, Kunze WAA, Thomas EA and Bertrand PP (1999) Long-term effects of synaptic activation at low frequency on excitability of myenteric AH neurons. *Neurosci.* 90:277–278.
- Destexhe A, Mainen ZF, Sejnowski TJ (1994) Synthesis of models for excitable membranes, synaptic transmission and neuromodulation using a common kinetic formalism. *J. Comput. Neurosci.* 1:195–230.
- Destexhe A, Sejnowski TJ (1995) G protein activation kinetics and spillover of gamma-aminobutyric acid may account for differences between inhibitory responses in the hippocampus and thalamus. *Proc. Natl. Acad. Sci. (USA)* 92:9515–9519.
- Furness JB, Costa M (1987) The Enteric Nervous System. Churchill Livingstone, Edinburgh.
- Galligan JJ, Tokimasa T, North RA (1987) Effects of three mammalian tachykinins on single enteric neurons. *Neurosci. Letters* 82:167–171.
- Gray PC, Scott JD, Catterall WA (1998) Regulation of ion channels by cAMP-dependent protein kinase and A-kinase anchoring protein. *Current Opinion in Neurobiol.* 8:330–334.
- Hempel CM, Vincent P, Adams SR, Tsien RY, Selverston AI (1996) Spatio-temporal dynamics of cyclic AMP signals in an intact neural circuit. *Nature* 384:166–169.
- Hille B (1992) Ionic Channels of Excitable Membranes (2nd ed.) Sinauer Associates, Sunderland, MA.
- Johnson PJ, Bornstein JC, Burcher E (1998) Roles of neuronal NK1 and NK3 receptors in synaptic transmission during motility reflexes in the guinea-pig ileum. *Br. J. Pharmacol.* 124 (7):1375–1384.
- Katayama Y, North RA (1978) Does substance P mediate slow synaptic excitation within the myenteric plexus? *Nature* 274:387–388.
- Kunze WAA, Furness JB, Bornstein JC (1993) Simultaneous intracellular recordings from enteric neurons reveal that myenteric AH neurons transmit via slow excitatory postsynaptic potentials. *Neurosci.* 55:685–694.
- Kunze WAA, Bertrand PP, Furness JB, Bornstein JC (1997) Influence of the mucosa on the excitability of myenteric neurons. *Neurosci.* 76:619–634.
- Kunze WAA, Furness JB (1999). The enteric nervous system and regulation of intestinal motility. *Ann. Rev. Physiol.* 61:117–124.
- Lamb TD (1996) Gain and kinetics of activation in the G-protein cascade of phototransduction. *Proc. Nat. Acad. Sci.* 93:556–570.
- Lamb TD, Pugh EN (1992) A quantitative account of the activation steps involved in phototransduction in amphibian photoreceptors. *J. Physiol.* 449:719–758.
- Morita K, Katayama K (1992) Substance P inhibits activation of

- calcium-dependent potassium conductances in guinea-pig myenteric neurones. *J. Physiol.* 447:293–308.
- Morita K, North RA (1985) Significance of slow synaptic potentials for transmission of excitation in guinea-pig myenteric plexus. *Neurosci.* 14:661–672.
- Naumoschat J, an der Heiden U (1997) A theoretical approach to G-protein modulation of cellular responsiveness. *Math. Biol.* 35:609–627.
- Nemeth PR, Palmer JM, Wood JD, Zafirov DH (1986) Effects of forskolin on electrical behaviour of myenteric neurones in guinea-pig small intestine. *J. Physiol.* 376:439–450.
- Pan H, Wang HY, Friedman E, Gershon MD (1997) Mediation by protein kinases C and A of Go-linked slow responses of enteric neurons to 5-HT. *J. Neurosci.* 17:1011–1024
- Press WH, Teukolsky SA, Vetterling WT, Flannery BP (1992) *Numerical Recipes in C: The Art of Scientific Computing* (2nd ed.). Cambridge University Press, Cambridge.
- Ross EM (1989) Signal sorting and amplification through G protein-coupled receptors. *Neuron* 3:141–152.
- Southwell BR, Woodman HL, Murphy R, Royal SJ, Furness JB (1996) Characterisation of substance P-induced endocytosis of NK1 receptors on enteric neurons. *Histochem. and Cell Biol.* 106:563–571.
- Taylor SS (1989) cAMP-dependent protein kinase: Model for an enzyme family. *J. Biol. Chem.* 264:8443–8446.
- Thomas EA, Bertrand PP, Bornstein JC (1999) Genesis and role of coordinated firing in a feed forward network: A model study of the enteric nervous system. *Neurosci.* 93:1525–?.
- Torre V, Ashmore JF, Lamb TD, Menini A (1995) Transduction and adaptation in sensory receptor cells. *J. Neurosci.* 15:7757–7768.
- Vergara C, Latorre R, Marrion NV, Adelman JP (1998) Calcium-activated potassium channels. *Current Opinions in Neurobiol.* 8(3):321–329.
- Wood JD (1994) Physiology of the enteric nervous system. In: Johnson LR, ed. *Physiology of the Gastrointestinal Tract*. Raven Press, New York. pp. 423–482.